Steel and Composite Structures, *Vol. 36, No. 1* (*2020*) *75-86*
DOI: https://doi.org/10.12989/scs.2020.36.1.075

Fatigue performance and life prediction methods research on steel tube-welded hollow spherical joint

Qi Guo[1], Ying Xing[1,2], Honggang Lei*[1], Jingfeng Jiao[1] and Qingwei Chen[3]

[1]*College of Civil Engineering, Taiyuan University of Technology, Taiyuan 030024, China*
[2]*College of Civil Engineering, Hunan University, Changsha 410082, China*
[3]*Economic & Technology Research Institute of State Grid Shandong Electric Power Company, Jinan 250021, China*

(*Received June 24, 2019, Revised June 3, 2020, Accepted June 17, 2020*)

Abstract. The grid structures with welded hollow spherical joint (WHSJ) have gained increasing popularity for use in industrial buildings with suspended cranes, and usually welded with steel tube (ST). The fatigue performance of steel tube-welded hollow spherical joint (ST-WHSJ) is however not yet well characterized, and there is little research on fatigue life prediction methods of ST-WHSJ. In this study, based on previous fatigue tests, three series of specimen fatigue data with different design parameters and stress ratios were compared, and two fatigue failure modes were revealed: failure at the weld toe of the ST and the WHSJ respectively. Then, S–N curves of nominal stress were uniformed. Furthermore, a finite element model (FEM) was validated by static test, and was introduced to assess fatigue behavior with the hot spot stress method (HSSM) and the effective notch stress method (ENSM). Both methods could provide conservative predictions, and these two methods had similar results. However, ENSM, especially when using von Mises stress, had a better fit for the series with a non- positive stress ratio. After including the welding residual stress and mean stress, analyses with the local stress method (LSM) and the critical distance method (CDM, including point method and line method) were carried out. It could be seen that the point method of CDM led to more accurate predictions than LSM, and was recommended for series with positive stress ratios.

Keywords: ST-WHSJ; fatigue; life prediction method; S-N curves; LSM; CDM

1. Introduction

As one of the major joints in grid structures, steel tube-welded hollow spherical joint (ST-WHSJ) have been widely used in industrial plants, large-span stadiums and aircraft maintenance facilities (Yang 2017), because of the advantages of low price, light weight, easy fabrication and convenient application, especially in China. For industrial plants and aircraft maintenance facilities, suspended cranes are often installed on grid structures to meet the requirements of industry (Zhang 2019), as shown in Fig. 1. However, with the increasing of load level of cranes, usage frequency, and service time, fatigue failure may occur in the ST-WHSJ (shown in Fig. 2), which is the fatigue critical part of this type of grid structures. In addition, fatigue failure of ST-WHSJ may also result in a progressive collapse, which may cause grave losses of life and property.

The static behavior of ST-WHSJ has been well studied through a large number of experiments. The formulas for calculating its ultimate axial tensile and compressive capacity were obtained by Han (2004). In addition, Liu (2018) proposed the bearing capacity of WHST with H-beam under axial stress, and revealed the post-fire residual mechanical behavior of WHSJ.

There are several cyclic loads during a crane lifting operation, which have a huge influences on grid structures. Therefore, it was suggested by the Technical Specification for Space Frame Structures (JGJ 7-2010, 2010) in China that fatigue tests should be carried out when the grid structure is subjected to suspended crane loads more than 5 $\times 10^4$ cyclic cycles.

The fatigue behavior of the bolt sphere joint another popular joint in large span structures, had been well studied. Yang (2017) obtained the S-N curves of M20 and M30 bolt sphere joints. Wang (2016) conducted a low cycle fatigue test of M12 and M16 bolted connections. Tizani (2014) researched on the fatigue life of an anchored blind bolt loaded in tension.

However, knowledge about the fatigue behavior of ST WHSJ has been developing relatively slowly, and only a few fatigue tests were obtained. Jiao (2018) conducted a series of tests on welded cross plate-hollow sphere joints, and found that specimens fractured at the weld toe of the cross plate and hollow sphere joint. Yan (2013) and Zhang (2018) carried out tests on ST-WHSJ, the difference between them is that the former specimens have a relatively strong tube, and the latter specimens have a relatively strong welded hollow spherical joint. S-N curves of spherical joint and tube nominal stress were obtained respectively for certain design parameters.

It is well known that design parameters and welding details can greatly affect fatigue performance (Pecnik 2019), while fatigue tests cannot be carried out to cover all possible cases due to the high economic and time costs.

*Corresponding author, Professor
E-mail: lhgang168@126.com

ISSN: 1229-9367 (Print), 1598-6233 (Online)

Therefore, fatigue life prediction methods are required. Fatigue life prediction techniques for metallic materials are comparatively mature, and have been reviewed by Santecchia (2016). However, the fatigue life prediction methods for welded joints are developing slowly. At present, there are some analytical approaches readily available, including the nominal stress method, the hot spot stress method and the effective notch stress method.

The nominal stress method is suggested by most design codes, including the International Institute of Welding (IIW 2016) and the Det Norske Veritas (DNV 2011), but this method is applied only to some standard welding details with sufficient test data. Unfortunately, there are no available fatigue classes for ST-WHSJ in any standards.

The hot spot stress method (HSSM) and the effective notch stress method (ENSM) were proposed by IIW and DNV and have also been widely accepted. HSSM and ENSM take advantage of the extrapolation stress of hot spot and notch stress with a 1mm notch radius respectively. Kim (2014) even expended its applied range to concrete filled circular hollow steel members. In addition, both methods take weld geometry into account, but their application in grid structures have not been validated yet.

Besides, proper and accurate methods for the fatigue assessment of welded joints are still urgent needed. Local stress method (LSM) and critic distance method (CDM) were established based on Neuber laws, which took the notch point and a certain distance from the notch as the evaluation criteria of fatigue behavior. Nominal stress method, HSSM, ENSM, and CDM were verified well to estimate lifetime of inclined cruciform welded specimens with simple models by Zamzami (2018). Li (2017) tried to assess the fatigue stresses and strains of countersunk riveted lap joint with LSM. However, these methods still face some limitations, which include the lack of "transferability" between experimental data obtained from different joint configurations with different levels of stress concentration and/or testing conditions (Bebera 2019). This transferability issue is often related to the difficulty of predicting the lifetime of samples with inhomogeneous stress distributions (i.e. stress concentrations conditions) such as ST-WHSJ. Besides, LSM and CDM do not taken the welding residual stress into consideration, which has a huge influence on ST-WHSJ.

Fig. 1 Grid structure with suspending cranes

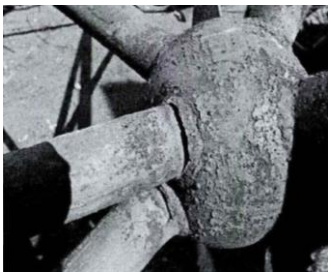

Fig. 2 Fatigue problem of ST-WHSJ in maintenance facilities

In this study, based on previous experiments, the fatigue failure mode of ST-WHSJ was summarized, and S-N curves for nominal stress were uniformed. After validating the finite element model by static tests on ST-WHSJ, predictions obtained by HSSM and ENSM were compared with fatigue results. In addition, LSM and CDM were induced and modified by mean stress and welding residual stress, and the accuracy of fatigue life prediction were compared and discussed.

2. Fatigue tests and results

2.1 Tests details

Fatigue tests of ST-WHSJ were carried out in previous work by Zhang (2019) and Yan (2013). There were two groups of specimens in Zhang (2019), named G1 and G2 (series G), and one group of specimens with low dispersion in Yan (2013), named KQ. Their test specimens were similar except a slight difference: specimens in Zhang (2019) consisted of steel tube-welded hollow spherical joint- steel tube, while specimens in Yan (2013) consisted of steel tube-welded hollow spherical joint- welded cross plate, as shown in Fig. 3. However, the difference had little influence on the fatigue performance.

The end of the steel tube was connected to the hollow sphere using manual electric arc welding. The specimen and welding details are shown in Fig. 4. The material used for the steel tube and the hollow sphere was Q235 B. For each group, design parameters, material properties and stress ratio R used in the test are listed in Table 1. All the material parameters and geometric parameters met the requirements of related standards in China.

2.2 Failure modes

Fatigue tests were conducted with MTS and AMSLER fatigue test machines with a frequency of 10 Hz and 6.67 Hz for series G and series KQ, respectively. The differences of frequency is small, so the influence was not taken into account.

The fractured specimens can be classified into two groups, as shown in Fig. 5. The series G, with a relatively strong WHSJ, fractured at the weld toe of steel tube, whereas the series KQ with a relatively strong steel tube, fractured at the weld toe of WHSJ.

Table 1 Design and mechanical parameters of specimen

Specimen Group	ST				WHSJ				*R*
	d(mm)	*t*(mm)	σ_y (MPa)	σ_u (MPa)	*D*(mm)	*T*(mm)	σ_y (MPa)	σ_u (MPa)	
G1	48	3.5	284	424	200	8	267	395	0
G2	60	3.5	290	472	200	8			0.4
KQ	127	8	-	-	400	10	-	-	0.3

Notes: *d* and *t* are the diameter and thickness of ST; *D* and *T* are the diameter and thickness of WHST, σ_y is yield stress and σ_u is ultimate stress

(a) Specimen type G1 and G2 (Zhang 2019)

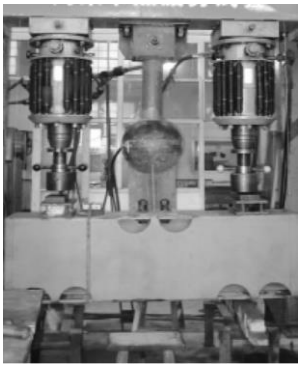

(b) Specimen type KQ (Yan 2013)

Fig. 3 Fatigue tests setup

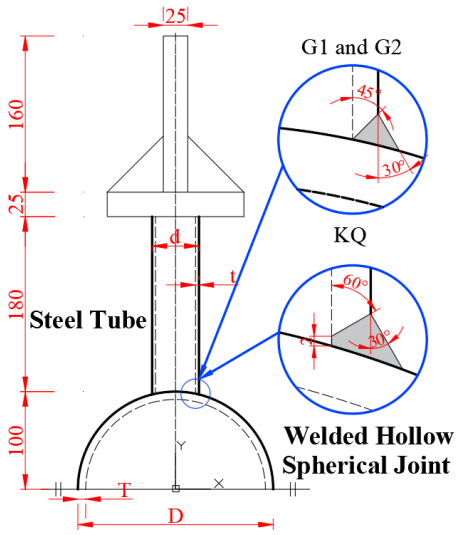

Fig. 4 Layout and welding details of specimens

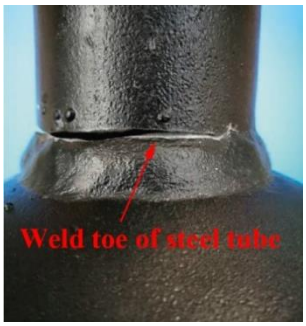

(a) Series G (Zhang 2019)

(b) Series KQ (Yan 2013)

Fig. 5 Fatigue failure positions

The fatigue fracture modes are revealed in Fig 6. As for series G, microcracks were initiated at the weld toe of the steel tube at first. With the load cycling, the microcracks coalesced and developed into macroscopic cracks. Then, the microcracks kept propagating and the macroscopic cracks kept growing along the radial and circumferential directions. At the same time, the number of crack increased. As a result, the net sectional area of the specimen decreased, and the specimen fractured due to the high local stresses at the crack tip, as shown in Fig. 6(a).

As for series KQ, it shared a similar fracture mode, and the main difference was that the crack was initiated at the weld toe of WHST rather than ST. It should be noticed that the crack still propagated along the radial direction rather than the vertical direction, as shown in Fig. 6(b).

2.3 S-N curves of nominal stress

Nominal stress of ST (Zhang 2019) and WHSJ (Yan 2013) was adopted in S-N curves respectively in previous work, so the stress was not comparable. In this paper, the stress was defined as the nominal stress of ST uniformly, so

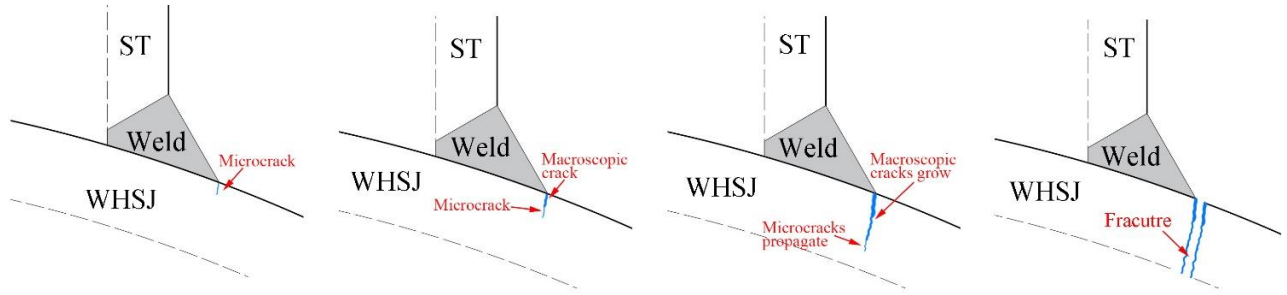

(a) Series G

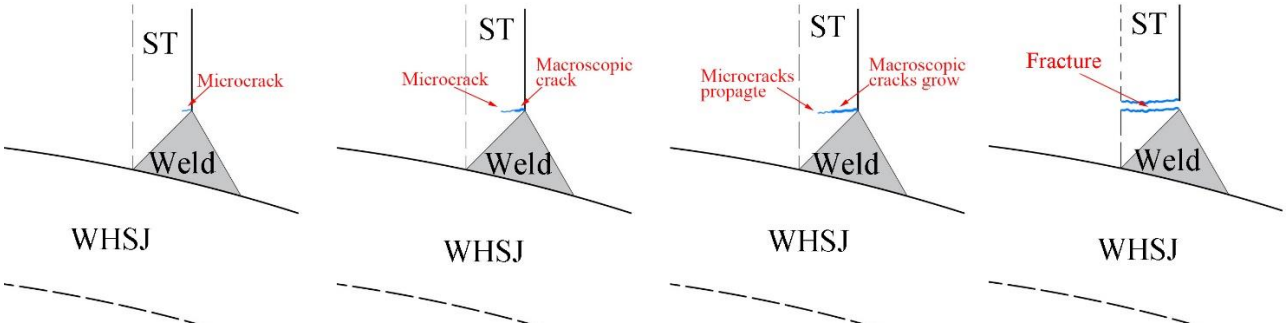

(b) Series KQ

Fig. 6 Fatigue failure modes

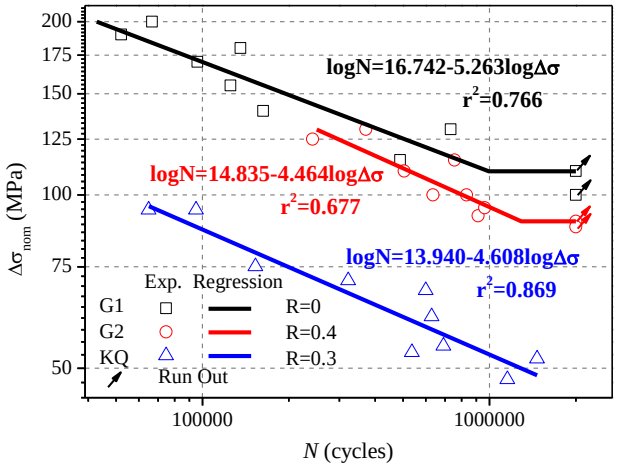

Fig. 7 S-N curves

that all S-N curves can be portrayed in a same figure. Therefore, cyclic loads were extracted and a new nominal stress was obtained for series KQ. Besides, fatigue data and S-N curves of series G with different stress ratios were separated by G1 and G2. As a result, new S-N curves of nominal stress were redrawn and regressed as in Fig. 7.

The test specimens were considered to have failed when obvious fatigue fracture occurred, and the deformation of the specimen reached the pre-set displacement limit. The arrow in Fig. 7 indicates the run out specimens, whose fatigue life was longer than 2×10^6 cycles, and considered not to fail in engineering practices.

It can be seen from Fig. 7 that the fatigue data were in good agreement with linear regression, and that the S-N curves were nearly paralleled to each other. As for G1 and G2, the curve of G2 was below that of G1, because the larger stress ratio *R* led to a shorter fatigue life. However, as the G1 and G2 curves are close, it seems that the influence of the stress ratio is limited for welded structures like ST-WHSJ. KQ curve was still below G2 curve. Despite its lower stress ratio, the KQ curve is below the G2 curve because of its different failure mode.

3. Finite element analysis (FEA)

In order to research different life prediction methods by finite element analysis, finite element models should be validated in the first place. Therefore, a finite element model (FEM) was established by *ABAQUS*, and compared with the static tests of ST-WHSJ. Due to the assumption of symmetry, the FEM can be simplified into a half ST-WHSJ, and then can also be simplified into a quarter of the ST-WHSJ (Yan 2013). The boundary of the bottom was set as fixed constraint, and the two sides of the model were set as symmetry constraints. The axial load of G1 and G2 was 20 kN and 30 kN respectively according to Zhang (2019), and then was applied as axial pressure at the top of steel tube, as shown in Fig. 8.

The material properties were defined as listed in Table 1, and the weld material was assumed to have the same properties. The elasticity modulus was taken as 206000N/mm^2. The mesh type was 8-node hexahedral element C3D8, and the mesh size were 2 mm and 8 mm in the refined mesh zone and non-refined mesh zone, respectively. The gauges arrangement and stress nephogram are shown in Fig. 9.

Table 2 Comparison of FEM results and test data

Gauge ID	G1					G2				
	Stress values(MPa)			Stress type	Error	Stress values(MPa)			Stress type	Error
	Test (Zhang 2019)	Average	FEA			Test (Zhang 2019)	Average	FEA		
P1	44.08	43.36	40.9	S33	5.68%	50.06	49.24	48.31	S33	1.88%
P2	42.64					48.41				
P3	44.29	43.57	41.16	S33	5.53%	50.47	49.13	48.36	S33	1.57%
P4	42.85					47.79				
P5	37.9	35.95	36.24	S33	0.82%	39.14	38.63	41.8	S33	8.21%
P6	33.99					38.11				
P7⊥	73.75	69.88	61.36	S_{csys}	12.19%	83.67	83.5	75.1	S_{csys}	10.06%
P8⊥	66.01					83.33				
P7 ‖	37.78	36.21	38.08	S22	5.18%	39.93	41.43	41.38	S22	0.10%
P8 ‖	34.63					42.92				
S1⊥	70.45	67.2	59.15	S_{csys}	11.97%	70.72	67.91	64.08	S_{csys}	5.64%
S2⊥	63.95					65.1				
S1 ‖	36.38	34.48	33.4	S22	3.12%	37.28	36.85	36.2	S22	1.76%
S2 ‖	32.57					36.42				
S3	3.09	3.19	3.17	S_{csys}	0.79%	7.62	7.42	7.83	S_{csys}	5.56%

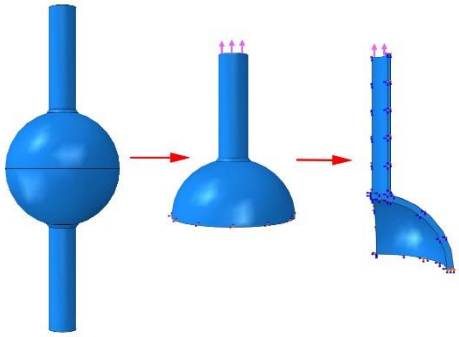

Fig. 8 Simplification of model

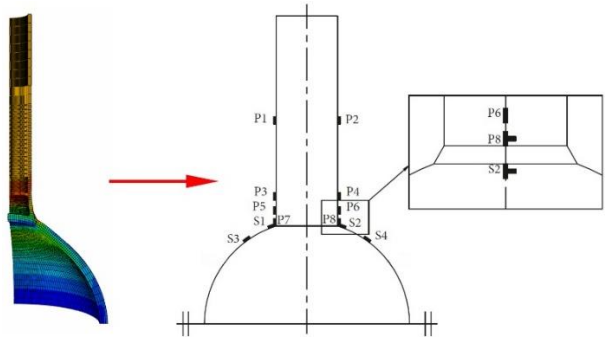

Fig. 9 Stress nephogram of FEM and gauges arrangement

Analysis results of FEM were compared with average stress measured in tests, as shown in Table 2. In this table, S33 and S22 stand for vertical and lateral stress in FEA.

The local coordinate systems should be established at the locations of P7⊥, P8⊥, S1⊥,S2⊥,S3 and S4 in post processing, and their principal axis are paralleled to the direction of the gauge. Then, the stress along this direction was taken as S_{csys} at this point.

It can be seen from the Table 2 that the FEA results and test data are in good agreement, all the errors are within 15%. Besides, the analysis results of series KQ compared similarly, so they were not included in the paper. Above all, the accuracy of the FEM was validated.

4. Discussions

4.1 Hot spot stress method (HSSM)

The hot spot stress method takes the stress concentration caused by dimensions and load parameters into consideration, and uses linear or quadratic extrapolation to obtain the reference point stress by IIW (2016) and DNV (2011). This method is limited to the cases for which the crack grows from the weld toe. Therefore, it is applicable for the series G and series KQ, which crack initiated at the weld toe of ST and WHSJ. The reference points on the surface of the hot spot stress are shown in Fig. 10.

The hot spot stress can be calculated with Eq. (1) and (2), and then transformed into K_{hs} using Eq. (3).

Linear extrapolation

$$\sigma_{hs}=1.67\sigma_{0.4\,t}-0.67\sigma_{1.0t} \quad (1)$$

(a) Linear extrapolation (b) Quadratic extrapolation

Fig. 10 Hot spot reference points

Quadratic extrapolation

$$\sigma_{hs}=2.52\sigma_{0.4\,t} - 2.24\sigma_{0.9t} + 0.72\sigma_{1.4t} \quad (2)$$

$$K_{hs} = \frac{\sigma_{hs}}{\sigma_{nom}} \quad (3)$$

Where σ_{hs} is hot spot stress; t is the thickness of the weak part, for series G and series KQ, it is the thickness of ST and WHSJ respectively; $\sigma_{0.4\,t}$, $\sigma_{1.0t}$, $\sigma_{0.9t}$ and $\sigma_{1.0t}$ are the stress values at reference points 0.4t, 0.9t, 1.0t and 1.4t away from the hot spot; K_{hs} is the stress concentration factor of the hot spot stress and σ_{non} is the nominal stress of ST.

It is known that the mesh size affects the FEM result to some extent. Thus, a parametric analysis was carried out about this factor, and the max principal stress was extracted from the FEM results to calculate K_{hs} by Eq. (1) - (3). Mesh type is same as FEM in section 3. The results are shown in Fig. 11.

It can be seen clearly that K_{hs} increases gradually as the mesh size decreases from t/2~ t/6, and that the difference between the increments were within 15%. However, K_{hs} was stable when the mesh size was smaller than t/6.

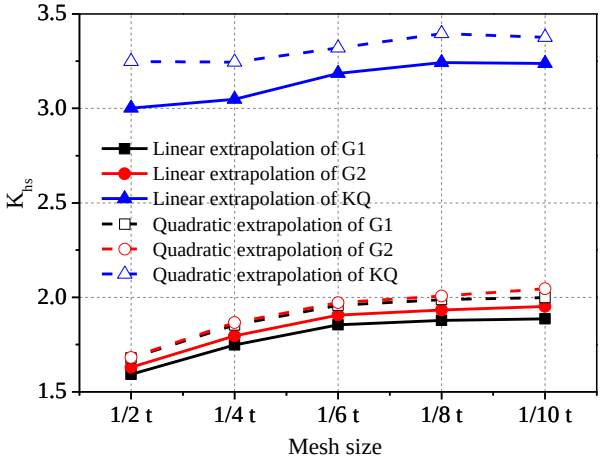

Fig. 11 Influence of mesh size

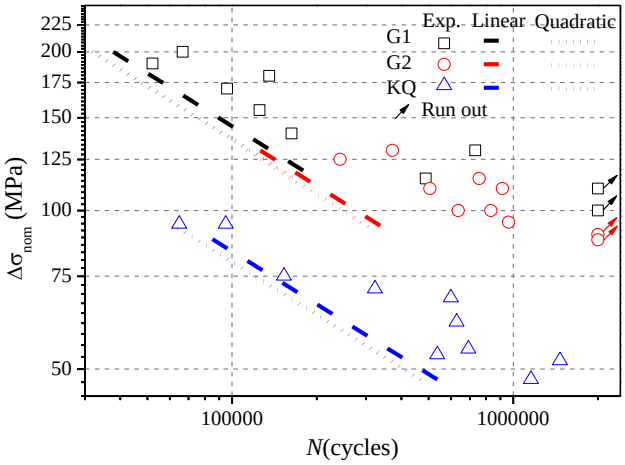

Fig. 12 S-N curves with HSSM

The results of quadratic extrapolation was 3%~7% larger than that of linear extrapolation. Therefore, taking both calculation precision and computational cost into consideration, a mesh size of t/8 was chosen in the following analysis with HSSM.

Despite linear extrapolation is closer to test date than quadratic extrapolation, it still cannot meet the requirement of accurate prediction

$$\log N = 12.301 - 3\log(K_{hs} \times \Delta\sigma_{nom}) \quad (4)$$

4.2 Effective notch stress method (ENSM)

The weld contour is not smooth; in fact, the chamfer of the weld toe and the gap between weld roots usually lead to a high stress concentration, which affects the initiation of fatigue crack. The effective notch stress uses the total stress including the influence of the notch at the root, and obtains linear-elastic material behavior. Statistics through a large number of tests showed that the weld contour can be replaced by an effective one with a notch radius of r=1mm (Radaj 2006), which was adopted by IIW. The notch stress is then used to assess the fatigue behavior by FEM. The element size is limited to be less than 0.15 mm and 0.25

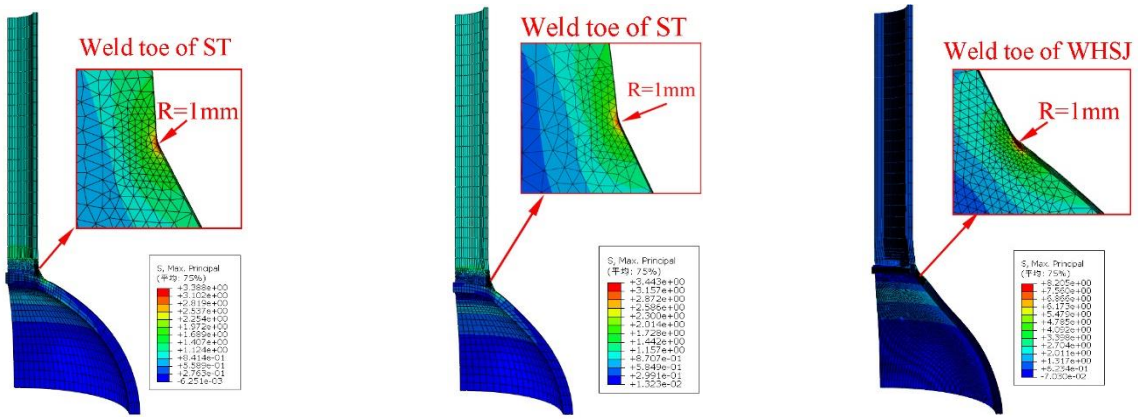

(a) G1 (b) G2 (c) KQ

Fig. 13 Analysis of the notch stress

mm for linear and quadratic elements, respectively (Fricke, 2012). The class of ENSM can be characterized as FAT 225 for max principal stress and FAT 200 for von Mises stress. Then, the formulas for fatigue life can be stated Eq. (5) - (7).

For max principal stress

$$\log N = 13.358 - 3\log(K_{ens,\,max} \times \Delta\sigma_{nom}) \tag{5}$$

For von Mises stress

$$\log N = 13.204 - 3\log(K_{ens,\,mises} \times \Delta\sigma_{nom}) \tag{6}$$

$$K_{ens} = \frac{\sigma_{ens}}{\sigma_{nom}} \tag{7}$$

Where K_{ens} is the stress concentration factor of the effective notch stress and σ_{ens} is the effective notch stress.

FEA was conducted on G1, G2 and KQ, as shown in Fig. 13. By applying a unit pressure on the top of tube, σ_{ens} and K_{ens} were obtained as listed in Table 3. As ST was the weak part of G1 and G2, their K_{ens} were similar, while KQ exhibited a much higher values because the stronger ST made the stress of the weaker WHST rise dramatically. K_{ens} were larger than K_{hs} in Fig. 11, because of considering the local stress of the notch.

Based on Eq. (5) - (7), S-N curves were obtained with ENSM, as shown in Fig. 14. All curves of ENSM-Max were below those of ENSM-Mises, and the ENSM-Mises ones were closer to the fatigue data. Compared with HSSM, ENSM provided a better fit for series G, and a worse fit for series KQ.

Table 3 K_{ens} from FEM

Series	Location of the notch	Max principal stress	Von Mises stress
G1	Weld toe of ST	3.888	3.279
G2	Weld toe of ST	3.443	2.952
KQ	Weld toe of WHSJ	8.205	7.082

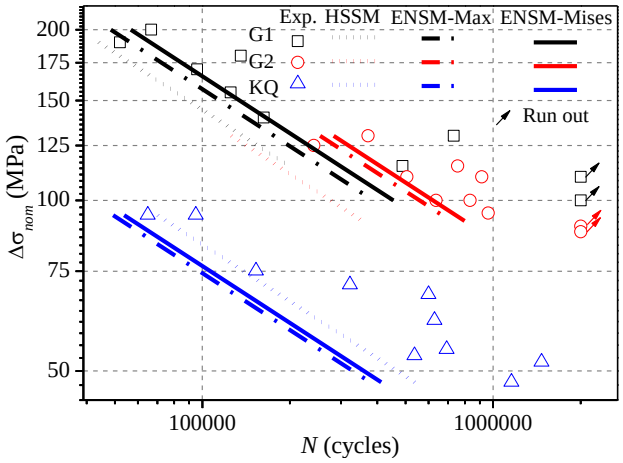

Fig. 14 S-N curves with ENSM

Notes: HSSM is the curves obtained by linear extrapolation with HSSM; ENSM-Max and ENSM-Mises are the curves obtained by max principal stress and von Mises stress with ENSM.

However, almost all the data were above their corresponding HSSM S-N curves. It indicates that the methods provided by IIW (2016) DNV (2011) provide safe values but cannot predict the fatigue life accurately, especially for G2 and KQ. The possible reasons are:

a)The S-N curves provided by IIW have a guaranteed rate above 90%, which leads to a conservative result;

b) IIW has no regard for the difference of welded materials, despite weld geometry influences the fatigue behavior primarily;

c) The welding residual stress and mean stress, which have a great influence on the fatigue performance, are not taken into account.

Therefore, ENSM and HSSM can predict the trend and a conservative result for ST-WHSJ. ENSM by Mises stress could provide an acceptable prediction of series G1. But for accurate prediction of series G2 and KQ, a refined analysis method is needed.

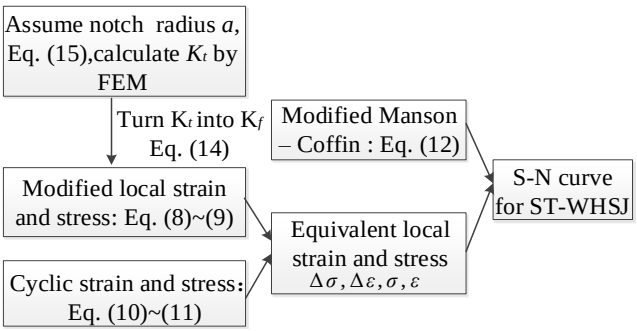

Fig. 15 Flow chart of LSM

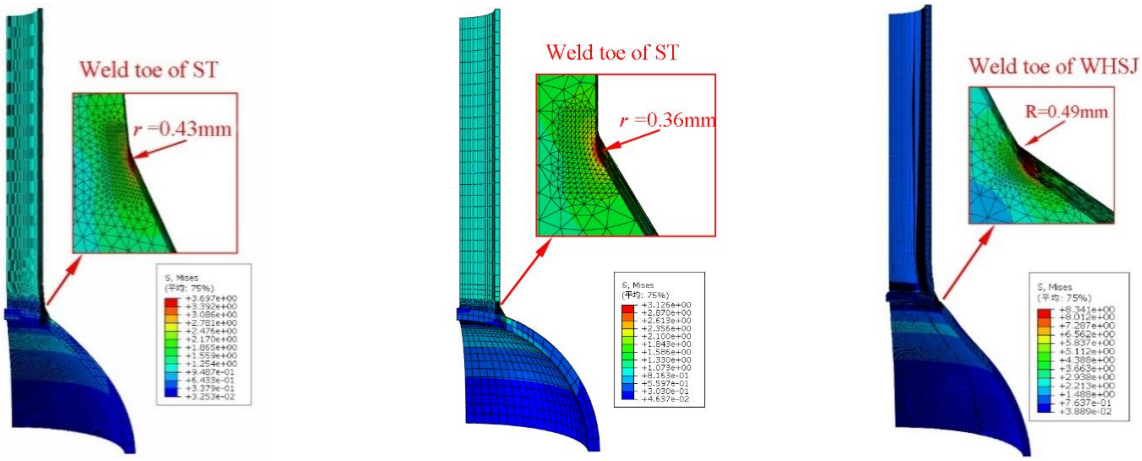

(a) G1 (b) G2 (c) KQ

Fig. 16 FEA with LSM

4.3 Local strain method (LSM)

LSM is a refined method which considers material plasticity to predict the fatigue life of welding details based on local strain at a stress concentration. It also should be noted that the residual stress of an initial notch in the weld can be considered in the local stress. The relationship between the local stress and strain thus becomes

$$\sigma\varepsilon = \frac{1}{E}(K_f \sigma_{nom} + \sigma_{res})^2 \tag{8}$$

Where σ and ε are the local stress and strain at the notch; E is the Young's modulus, 206000 MPa for Q235 steel; K_f is the fatigue notch factor; σ_{nom} is the nominal stress; σ_{res} is the welding residual stress.

Wang (2018) conducted welding residual stress analysis on ST-WHSJ, and found out the max residual stress was 204 MPa which was close to the steel grade of Q235 (235MPa). Besides, Beretta (2009) directly assumed the residual stress to be as high as the tensile yield stress. Thus, σ_{res} was chosen to be the yield stress (235MPa) of Q235 steel for safety. Then the Neuber formula was modified to include the stress ratio, as shown in Eq. (9).

$$\Delta\sigma\Delta\varepsilon = \frac{1}{E}\left(\frac{K_f \Delta\sigma_{nom}}{1-R}\right)^2 \tag{9}$$

Where Δσ and Δε is the stress range of local stress and strain; $\Delta\sigma_{nom}$ is the stress range of nominal stress; R is the stress ratio.

The relationships between the cyclic stress and strain are listed in Eq. (10) and (11).

$$\varepsilon = \frac{\sigma}{E} + \left(\frac{\sigma}{k}\right)^{\frac{1}{n'}} \tag{10}$$

$$\frac{\Delta\varepsilon}{2} = \frac{\Delta\sigma}{2E} + \left(\frac{\Delta\sigma}{2k}\right)^{\frac{1}{n'}} \tag{11}$$

in which k and n' are the cyclic strain hardening coefficient and exponent respectively.

Morrow modified the Manson–Coffin relationship by taking the effect of mean stress into account. In addition to the welding residual stress, the Manson–Coffin can be stated as Eqs. (12) and (13)

$$\varepsilon_a = \frac{\sigma_f^{'} - \sigma_m}{E}(2N_f)^b + \varepsilon_f^{'}(2N_f)^c \quad (12)$$

$$\sigma_m = \frac{\sigma_{max} + \sigma_{min}}{2} + \sigma_{res} \quad (13)$$

Where ε_a is the strain amplitude, equals to half of the strain range; $\sigma_f^{'}$ and $\varepsilon_f^{'}$ are the fatigue strength coefficient and the fatigue ductility coefficient, b and c are the fatigue strength exponent and fatigue ductility exponent, σ_m is the mean stress at the notch; σ_{max} and σ_{min} are the maximal and minimum notch stresses in a cyclic load.

K_f can be calculated from the notch stress concentration factor K_t through Peterson's formula (Lawrence 1981), as shown in Eq. (14), in which parameter a is related to the material properties. The value of a can be expressed as a function of the ultimate tensile strength by Eq. (15).

K_f reaches a maximum value with a notch radius equal to a and a "worst case" analysis can then be conducted by assuming a hypothetical notch radius r equal to a and applying Eq. (14) to obtain $K_{f,\max}$, the maximum value of K_f over r. The process of LSM can be simplified into a flow chart, as shown in Fig. 15.

$$K_f = 1 + \frac{K_t - 1}{1 + \frac{a}{r}} \quad (14)$$

$$a = 0.0254\left(\frac{2068}{\sigma_u}\right)^{1.8} \quad (15)$$

According to Eq. (15) and the ultimate stress value listed in Table 1, a notch radius of 0.43 mm, 0.36 mm at weld toe in ST, and 0.49mm at weld toe in WHSJ, were adopted and established in the FEM as the worst case. The mesh size was set to be 1/10 of the notch radius, as suggested by Beretta (2009). A unit nominal load was applied, and the local stressresults and values of K_t for these three welding details were obtained by FEA, as shown in Fig. 16. K_t at the weld root and weld toe were calculated as shown in Table 4, based on which K_f was obtained by Eq. (14).

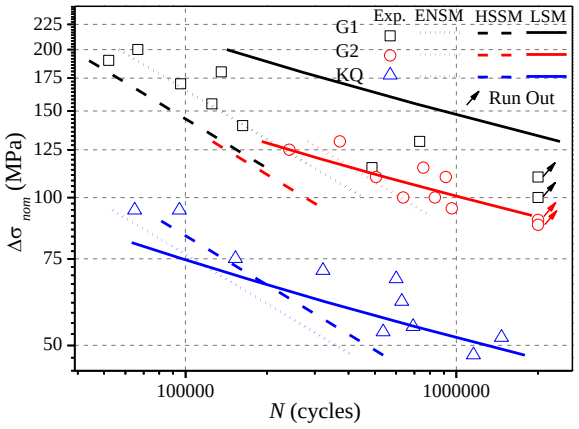

Fig. 17 S-N curves with LSM

Notes: ENSM stands for the curves obtained by von Mises stress with ENSM, HSSM is the curves obtained by linear extrapolation with HSSM.

Table 4 K_t and K_f for the three types of ST-WHSJ

Series	G1	G2	KQ
K_f	2.349	2.063	4.671

Table 5 Cyclic elastoplastic and fatigue properties of Q235 steel

Material	k' MPa	n'	σ'_f MPa	b	ε'_f	c
Q235 (Luo 2012)	999	0.1992	618	-0.0800	0.1559	-0.4620

For ST-WHSJ, material parameters are listed in Table 5. With these parameters, based on the flow chart in Fig. 15, the fatigue life predicted by LSM is compared to the test result in Fig. 17 for the three series. The fatigue life vs. nominal stress amplitude curves obtained by the LSA are in acceptable agreement with the test results, especially for series G2 and KQ, which provided a better solution than HSSM and ENSM. As such, the applicability of LSM was verified for the fatigue life prediction of ST-WHSJ. As for G1, with a stress ratio R=0, the S-N curve is above the fatigue data, which meant that the LSA had a lower predictive capability of non-positive stress ratio. Based on this evidence, LSM can only be recommended for welded structures like ST-WHSJ for positive stress ratios.

4.4 Critical distance method (CDM)

The critical distance method is based on the theory of critical distances (TCD) which proposes a unifying concept for averaging to assess fracture in both static and fatigue conditions (Tayor 2007). All these TCD methodologies employ a characteristic material length parameter, the critical distance (L), when performing fracture and fatigue assessments. Hence, with the support of FEA, the point method (PM) and the line method (LM) were implemented to assess the fatigue behaviour of ST-WHST, as shown in Fig. 18.

PM establishes that fracture occurs when the stress at a distance of $L/2$ from the notch tip is equal to the inherent strength. The effective stress of PM is then expresses as Eq. (16). LM considers the average stress over some distance from the notch tip, the effective stress of LM is shown in Eq. (17).

$$\sigma_{eff}^{PM} = \sigma(r = \frac{L}{2}, \theta = 0) \quad (16)$$

$$\sigma_{eff}^{LM} = \frac{1}{2L}\int_0^{2L} \sigma(r)dr(\theta = 0) \quad (17)$$

Where σ_{eff}^{PM} and σ_{eff}^{LM} are the effective stress of PM and LM; r is the distance from the notch and θ is the direction of the stress gradient.

The critical distance L is a material characteristic and is independent from the notch geometry. The critical distance can be calculated from the threshold stress intensity factor range ΔK_{th} and the full range of the specimen fatigue limit

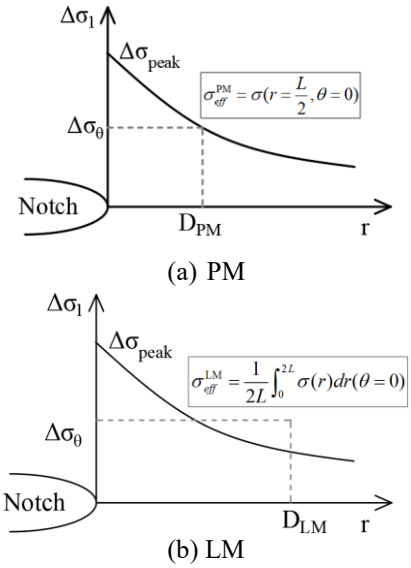

Fig. 18 Calculation of effective stress according to the TCD

$\Delta\sigma_f$, as shown in Eq. (18). The material characteristic length to be used to address static problems can also be defined as Eq. (19) (Taylor 2004).

$$L=\frac{1}{\pi}\left(\frac{\Delta K_{th}}{\sigma_f}\right)^2 \tag{18}$$

$$L_s=\frac{1}{\pi}\left(\frac{K_{IC}}{\sigma_u}\right)^2 \tag{19}$$

Where K_{IC} is the plane strain material toughness, and equals to 191.4 $\mathrm{MPa}\sqrt{\mathrm{m}}$ for Q235.

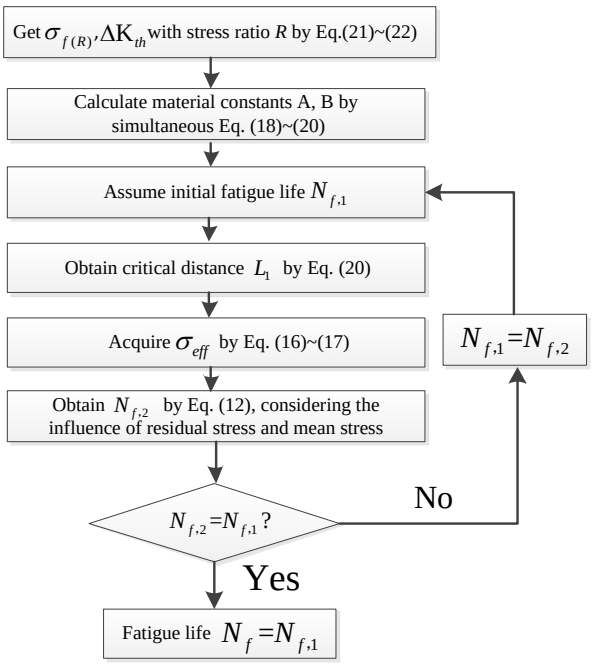

Fig. 19 Flow chart of calculating fatigue life with CDM

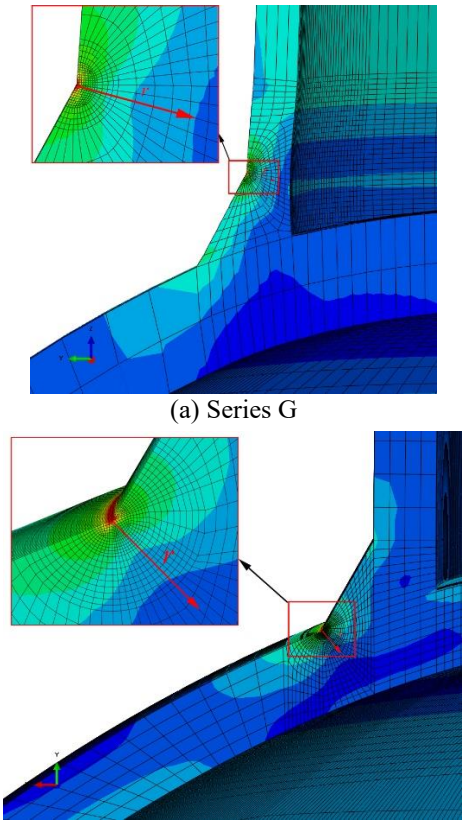

Fig. 20 Focus path based on TCD

Susmel (2007) hypothetized that the fatigue life is a power function of the applied stress, which was proven valid, as shown in Eq. (20).

$$L(N_f)=AN_f^B \tag{20}$$

Where A and B are constants, which are expected to be different for different materials and different stress ratios.

Benedetti (2019) emphasized the influence of the mean stress σ_m on ΔK_{th} and σ_f when combining the TCD. For different stress ratios of Q235 steel, σ_f and ΔK_{th} can be calculated by Geber's (Schijve 2009) suggestions, as shown in Eq. (21) and (22).

$$\frac{\sigma_{f(R)}}{\sigma_{-1}}=1-\left(\frac{\sigma_m}{\sigma_u}\right)^2 \tag{21}$$

$$\Delta K_{th}=\Delta K_{th0}(1-R)\gamma \tag{22}$$

Where $\sigma_{f(R)}$ and σ_{-1} are the fatigue limits with stress ratios R and -1 respectively, σ_{-1} was 160MPa as mentioned. γ is a material parameter, and its value is 0.71 for low-carbon steel Q235. ΔK_{th0} is ΔK_{th} for a stress ratio of R=0. ΔK_{th} equals to 7.137 $\mathrm{MPa}\sqrt{\mathrm{m}}$ with R=0.1, so ΔK_{th0} can be calculated to be 11.169 $\mathrm{MPa}\sqrt{\mathrm{m}}$ according to Eq. (22). The ultimate stress of ST and WHST are listed in Table 1.

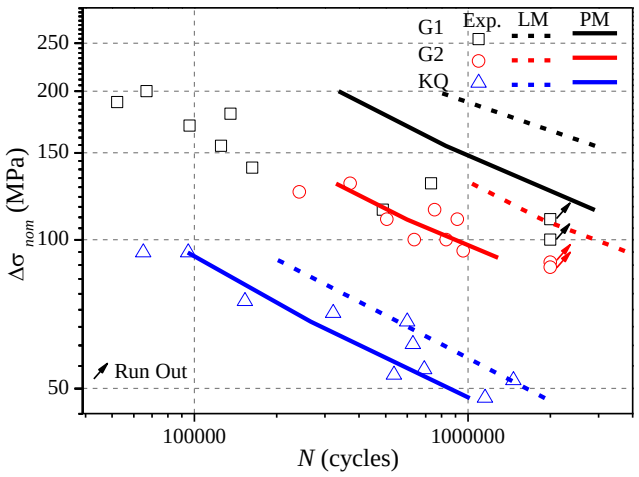

Fig. 21 S-N curves with PM and LM

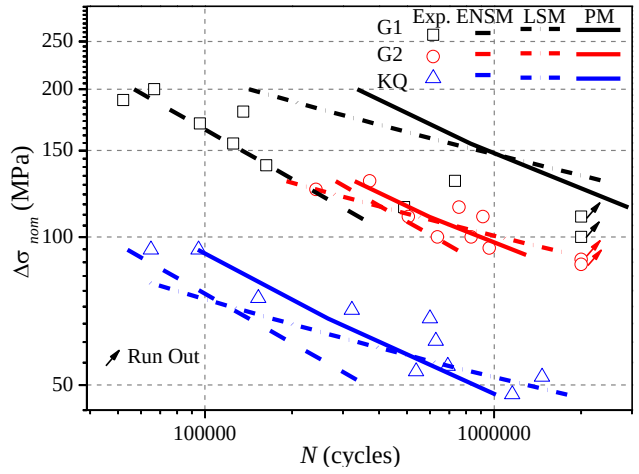

Fig. 22 Comparison of different methods

Notes: ENSM stands for the curves obtained by von Mises stress with ENSM.

Table 6 Fracture and fatigue parameters of three series

Series	R	$\sigma_{f(R)}$ MPa	ΔK_{th} MPa$\sqrt{m}$	A	B
G1	0	144.917	7.930	36.927	-0.252
G2	0.4	111.440	4.758	35.362	-0.283
G3	0.3	114.019	5.551	50.082	-0.289

Therefore, analysis can be carried out according to the flow chart of CDM in Fig. 19. L and L_s stand for the critical distance for static strength and fatigue limit respectively, and can be calculated to be constants according to Eq. (18) and (19) respectively. Loading cycles (N_f in Eq. (20)) for static strength were considered to be 1/4, and were taken as 2×10^6 cycles for fatigue limit in engineering practices. Combining the calculated values of L, L_s and 1/4, 2×10^6 with Eq. (20), material parameters A and B were obtained.

The material constants A and B were obtained for each series with different stress ratios, as shown in Table 6. Further, the so called focus path, the stress gradient direction, is recommended as being taken coincident with the notch bisector (Louks 2014), then the focus path was chosen for series G and KQ, as shown in Fig. 20. Afterwards, the nominal stress vs. fatigue life curves were acquired with PM and LM, as shown in Fig. 21. It can be seen from the figure that curves obtained with PM match the test data well, apart from series G1. As for G1, it is expected to occupy a longer fatigue life with a non-positive stress ratio. However, specimens seemed more sensitive to the welding defects, which reduced the fatigue capacity, and resulted in a significant decrease of fatigue life. That is to say, due to the non-positive stress ratio, the predictions by TCD tends to be hazardous for welded structures like ST-WHSJ. Besides, PM provides a better result than LM because LM takes an average of the stresses within the critical distance, which lowers the effective stress and leads to a longer predicted life.

The best curves in each method were chosen and are compared in Fig. 22. The figure indicates that both PM and LSM are in good agreement with test data for the series G2 and KQ which has a positive stress ratio, and it is obvious that PM has a more accuracy prediction. As for G1 with a non-positive stress ratio, ENSM by von Mises can provide an acceptable prediction.

5. Conclusions

Fatigue performance and life prediction methods on ST-WHSJ were studied in this paper. Fatigue tests of 30 specimens for three series with stress ratio of 0, 0.4 and 0.3 were summarized. Fatigue fracture modes were classified, and S-N curves of nominal stress were uniformed for each series.

Furthermore, after validating the FEM by static tests on ST-WHSJ, HSSM was carried out with linear and quadratic extrapolation, and the mesh size of HSSM was discussed. ENSM was conducted by max principal stress and von Mises stress individually. In addition, cyclic strain stress relationships and Manson–Coffin formulas were modified to include welding residual stress and mean stress, and then introduced into LSM and TCD to predict the fatigue life for three series. The results obtained from the analysis led to the following conclusions:

•The fatigue fracture modes of ST-WHSJ can be divided into two sorts: cracks initiating at the weld toe of ST (series G) and WHSJ (series KQ) respectively, and propagating along its radial direction.

•The S-N curves of nominal stress of the three series were uniformed and updated. In addition, FEM was validated by static tests, and the accuracy was above 85%.

•Both HSSM and ENSM can provide conservative predictions, while ENSM, especially when obtained by von Mises stress, had an acceptable fit for series G1, but a less one for series G2 and KQ. The mesh size of HSSM was suggested to be 1/8 of the thickness.

•After modified by welding residual stress and mean stress, the fatigue life was predicted with LSM, PM and LM. Both LSM and PM fit the test date well, while PM had more accurate predictions for series G2 and KQ, and a hazardous one for series G1.

•As for ST-WHSJ with positive stress ratios, PM was suggested to assess the fatigue strength. However, for that with a non- positive stress ratios, ENSM by von Mises stress is recommended.

Acknowledgments

The work in this paper was supported by the National Natural Science Foundation of China (No. 51708384), Natural Science Foundation of Shanxi Province, China (No.201801D221216 and No.201901D211017), Science & Technology Project of State Grid Shandong Electric Power Company (No. 52062519001A), and Science & Technology Project for Oversea Scholars in Shanxi Province (No. DC1900000602).

References

Bebera V.C., Schneidera B. and Bredea M. (2019), "Efficient critical distance approach to predict the fatigue lifetime of structural adhesive joints", Eng. Fract. Mech., in press. 10.1016/j.engfracmech.2019.03.022.

Beretta, S., Bernasconi, A. and Carboni, M. (2009), "Fatigue assessment of root failures in HSLA steel welded joints: a comparison among local approaches", *Int. J. Fatigue*, **31**, 102-110. 10.1016/j.ijfatigue.2008.05.027.

Benedetti, M. and Santu,s C. (2019), "Mean stress and plasticity effect prediction on notch fatigue and crack growth threshold, combining the theory of critical distances and multiaxial fatigue criteria", *Fatigue Fract. Eng. Mater. Struct.*, **42**(6), 1228-1246. 10.1111/ffe.12910.

Det Norske Veritas (2011), *Fatigue design of offshore steel structures*. Recommended practice DNV-RP-C203.

International Institute of Welding (2016), *Recommendations for fatigue design of welded joints and components*, IIW Joint Working Group, 2nd IIW-2259-15.

Fricke, W. (2012), *IIW Recommendations for the fatigue assessment of welded structures by notch stress analysis*, Woodhead Publishing Limited, UK.

Han, Q.H. and Liu, X.L. (2004), "Ultimate bearing capacity of the welded hollow spherical joints in spatial reticulated structures," *Eng. Struct.*, **26**(1), 73-82. 10.1016/j.engstruct.2003.08.012.

JGJ 7-2010 (2010), *Technical Specification for Space Frame Structures*, Ministry of Housing and Urban-Rural Construction of China, Beijing, Beijing, China. (in Chinese)

Jiao J.F., Lei, H.G. and Chen Y.F. (2018), "Numerical simulation and experimental study on constant amplitude fatigue behavior of welded cross plate-hollow sphere joints", *J. Southeast Univ. (Engl. Ed.)*, **34**(1), 62-70. 10.3969/j.issn.1003-7985.2018.01.010.

Kim I.J., *et al*. (2014), "Stress concentration factors of N-joints of concrete-filled tubes subjected to axial loads", *Int. J. Steel Struct*., **14**(1), 1-11. 10.1007/s13296-014- 1001-9

Lawrence, F.V., Ho, N.J. and Mazumdar, P.K. (1981), "Predicting the fatigue resistance of welds", *Annu. Rev. Mater. Sci.*, **11**, 401-425.

Li G., *et al*. (2017), "A methodology for assessing fatigue life of a countersunk riveted lap joint", *Adv. Aircr. Spacecr. Sci*., **4**(1), 1-https://doi.org/10.12989/aas.2017.4.1.001.

Liu H.B., *et al.* (2018), "Ultimate tensile and compressive performances of welded hollow spherical joints with H-beam", *J. Constr. Steel. Res.*, **150**, 195-208. 10.1016/j.jcsr.2018.08.018.

Louks R., Gerin B., Draper J., Askes H. and Susmel L. (2014), "On the multiaxial fatigue assessment of complex three-dimensional stress concentrators", *Int. J. Fatigue*, **63**,12-24. 10.1016/j.ijfatigue.2014.01.001.

Luo, Y., Wang, Q., Liu, Y. and Huang, C. (2012), "Low cycle fatigue properties of steel structure materials Q235 and Q345", *J. Sichuan Univ., Eng. Sci. Ed.*, **44**(2), 169-175. (in Chinese). 10.15961/j.jsuese.2012.02.012.

Pecnik, M., Nagode, M. and Seruga, D. (2019), "Influence of geometry and safety factor on fatigue damage predictions of a cantilever beam", *Struct. Eng. Mech*., **70**(1), 33-41. https://doi.org/10.12989/sem.2019.70.1.033.

Radaj, D. and Sonsino, C. (2006) *Fatigue Assessment of Welded Joints by Local Approaches*, Hamburg University of Technology, Germany.

Santecchia E., *et al*. (2016), "A review on fatigue life prediction methods for metals", *Adv. Mater. Sci. Eng.*, **2016**, 1-26. 10.1155/2016/9573524

Schijve J. (2009) *Fatigue of Structures and Materials (Second Edition)*, Springer, Dordrecht.

Susmel, L. and Taylor, D. (2007), "A novel formulation of the theory of critical distances to estimate lifetime of notched components in the medium-cycle fatigue regime", *Fatigue Fract. Eng. Mater. Struct.*, **30**(7), 567-581. 10.1111/j.1460-2695.2007.01122.x.

Taylor, D. (2004), "Predicting the fracture strength of ceramic materials using the theory of critical distances", *Eng. Fract. Mech.*, **71**, 2407-2416. 10.1016/j.engfracmech.2004.01.002.

Taylor, D. (2007) *The Theory of Critical Distances: A New Perspective in Fracture Mechanics*. Elsevier Science.

Tizani, W., Rahman, N.A. and Pitrakkos, T. (2014), "Fatigue life of an anchored blind-bolt loaded in tension", *J. Constr. Steel Res.*, **93**, 1-8. 10.1016/j.jcsr.2013.10.002.

Wang F., Tian S.J. and Lei H.G. (2018), "Impact analysis of residual stress on fatigue strength of steel pipe-welded hollow spherical joints", *Build. Struct.*, **48**(1), 456-460. 10.19701/j.jzjg.2018.s1.105.

Wang, Z., Wang, Q., Xue, H. and Liu, X. (2016), "Low cycle fatigue response of bolted T-stub connections to HSS columns - Experimental study", *J. Constr. Steel Res.*, **119**, 216-232. 10.1016/j.jcsr.2015.12.009

Yan, Y.J. (2013), "The analysis and testing study on fatigue properties of the steel pipe-welded hollow spherical joints in space latticed structure", Ph.D. Dissertation, Taiyuan University of Technology, China. (in Chinese)

Yang, X. and Lei, H.G. (2017), "Constant amplitude fatigue test of high strength bolts in grid structures with bolt-sphere joints", *Steel Compos. Struct*., **25**(5), 571-579. https://doi.org/10.12989/scs.2017.25.5.571.

Zamzami I.A. and Susmel L. (2018), "On the use of hot-spot stresses, effective notch stresses and the point method to estimate lifetime of inclined welds subjected to uniaxial fatigue loading", *Int. J. Fatigue*, **117**, 432–449. 10.1016/j.ijfatigue.2018.08.032.

Zhang J.L., Lei, H.G. and Jin, S.H. (2019), "Experimental study on constant-amplitude fatigue performance of weld toe in steel tube of welded hollow spherical joints in grid structures", *Adv. Mater. Sci. Eng.*, **2019**, 1-12. 10.1155/2019/6204302.

CC